Nature Environment and Pollution Technology
An International Quarterly Scientific Journal

p-ISSN: 0972-6268
(Print copies up to 2016)
e-ISSN: 2395-3454

Vol. 25 | No. 1 | Article ID B4331 | 2026

Original Research Paper

https://doi.org/10.46488/NEPT.2026.v25i01.B4331

Open Access Journal

Development of Zinc Oxide-Sawdust Composite Adsorbent for Methylene Blue Removal: Synthesis, Characterization and Adsorption Mechanism

Romit Antil and Anil K. Berwal†

Centre of Excellence for Energy and Environmental Studies, Deenbandhu Chhotu Ram University of Science & Technology, Murthal, Sonipat-131039, Haryana, India

†Corresponding author: Anil K. Berwal; romit.antil2@gmail.com

Abbreviation: Nat. Env. & Poll. Technol.
Website: www.neptjournal.com

Received: 08-04-2025
Revised: 28-05-2025
Accepted: 29-05-2025

Key Words:

Zinc oxide-sawdust composite
Zinc oxide nanocomposite
Methylene blue removal
Adsorption

Citation for the Paper:

Antil, R. and Berwal, A.K., 2026. Development of zinc oxide-sawdust composite adsorbent for methylene blue removal: Synthesis, characterization, and adsorption mechanism. *Nature Environment and Pollution Technology*, 25(1), B4331. https://doi.org/10.46488/NEPT.2026.v25i01.B4331

Note: From 2025, the journal has adopted the use of Article IDs in citations instead of traditional consecutive page numbers. Each article is now given individual page ranges starting from page 1.

ABSTRACT

The natural world provides sawdust, also known as wood shavings, which is a reasonably abundant and affordable lignocellulosic compound. It is a waste product of agriculture and industry that is abundant and has disposal issues. A zinc oxide nanocomposite based on sawdust (ZnO@SD) was synthesized to efficiently remove the dye methylene blue (MB) from aqueous solutions. FTIR, SEM, TEM, and XRD analyses were used to characterize the freshly made sawdust material. Batch optimization of adsorption experimental parameters, including initial dye concentration, contact time, solution pH, temperature, and adsorbent dosage used, to achieve the maximum removal of MB dye from wastewater. For an initial MB dye concentration of 50 mg/L, the ideal parameters for the maximum removal of MB dye from aqueous solution were determined to be: 40 mg of adsorbent, 80 minutes of contact time, a pH of 6.0, and 25°C. The models that best fit the examined experimental data were the Freundlich and pseudo-second order. For the removal of MB dye, the experimental adsorption capacity of ZnO@SD was found to be 372.5 mg/g. According to the obtained results, the sawdust composite was thought to be a low-cost and efficient adsorbent for dye removal.

INTRODUCTION

All living organisms depend upon water for their survival and growth. Nowadays, the improved lifestyle, industrialization, as well as urbanization cause water contamination at a higher rate. Water contamination has worsened due to a number of factors, such as the discharge of agricultural as well as domestic waste and the presence of huge industrial residues in water bodies. Urbanization and industrialization have a significant impact on water quality because their effluents are highly contaminated with both organic and inorganic pollutants. As the industrial sector has grown, including rubber, wood, textile, and dye industries, the amount of untreated wastewater that is released into streams and water bodies has also increased (Yadav et al. 2023).

Among the pollutants found in wastewater, dyes in particular can cause major health issues for individuals because of their carcinogenicity, mutagenicity, and toxicity, even at lower concentrations. These pollutants include organic dyes, such as methylene blue (MB), which is present in high concentrations in wastewater from a variety of industries, such as the production of paper, textiles, paint, and wool (Prodjosantoso et al. 2025). Methylene blue is a synthetic dye that is highly soluble and one of the most widely used dyestuffs. The MB dyestuff contributes to increased ecosystem pollution and has detrimental effects on microbes, humans, and animals (Khan et al. 2022). As it causes a negative impact on the process of photosynthesis, the chemical and biological oxygen demands, and the quantities

of oxygen required, it impacts the entire aquatic environment and harms human health (Ahamad & Nasar 2024).

Furthermore, because of their chemical stability, they are extremely resistant to light, aerobic digestion, as well as oxidizing agents (Bo et al. 2021). As a result, wastewater treatment is crucial, and a variety of technologies, including biochemical degradation, photocatalytic, electrocoagulation, oxidative, and adsorption methods, have been used for dye removal (Pimental et al. 2023, Dutta et al. 2021). The majority of these techniques have demonstrated their suitability in treating dye-contaminated water at laboratory scales, but they have limitations when it comes to large-scale relevance because they are expensive, require a lot of energy and time, and produce large amounts of secondary sludge (Bulgariu et al. 2019, Yadav et al. 2023).

Therefore, choosing a suitable approach has always been difficult. Among the various methods, the adsorption technique has drawn a lot of interest because it is less harmful, more affordable, simpler, more flexible, and less sensitive to harmful pollutants. Additionally, this method offers adsorbent recovery and minimal sludge generation and disposal issues (Yadav et al. 2024a).

One of the recently utilised adsorbents is bio-waste and its transformation into valuable materials for specific uses. As a bio-waste from industry and agriculture, sawdust is a cheap and plentiful lignocellulosic material. In addition to different extractives (acids, soluble sugars, resins, waxes, oils, etc.), its primary constituents are cellulose, lignin, and hemicellulose. Sawdust modification enhances its ability to absorb contaminants. Therefore, various materials, such as organic compounds, basic solutions, or acidic solutions, can be used to modify it. In order to remove dyes from wastewater, metal oxides have been widely employed as promising adsorbents. Zinc oxide nanoparticles are used extensively in gas sensors, energy storage, and solar cells. Due to its high adsorptive capacity for a variety of pollutants, ZnO NPs have attracted a lot of attention in wastewater treatment (Cao et al. 2024, Yadav et al. 2024b).

According to numerous studies, ZnO NPs have shown promise as adsorbents for organic dyes (Sayed et al. 2024). A study conducted by Zafar et al. (2019) found that the Langmuir adsorption model and the pseudo-second-order kinetic model were used to fit the adsorption of amaranth (AM) and methyl orange (MO) onto ZnO NPs. A pH of 6.0 was found to yield the highest adsorption capacities. Zhang et al. (2016) reported that ZnO NPs demonstrated higher adsorption ability towards anionic dyes such as Congo red (CR) and acid fuchsin (AF), as well as the cationic dye malachite green (MG). For CR, AF, and MG, the maximum adsorption capacities were 1554 mg/g, 3307 mg/g, and 2963 mg/g, respectively. The present study aims to synthesise ZnO NPs distributed in AC made from wood sawdust (ZnO@SD composite) for MB dye adsorption. The parameters influencing the adsorption performance, including solution pH, contact duration, adsorbent dosage, and initial dye concentration, were thoroughly examined. Kinetic, isotherm, and thermodynamic properties were also examined.

MATERIALS AND METHODS

SD was used as a precursor after being gathered from a nearby sawmill. Distilled water was used to wash away any contaminants that may have adhered to the wood sawdust. It was then ground and sieved after being dried for 24 hours at 100°C in an oven. Direct pyrolysis was used to produce biochar from SD, and a muffle furnace was used to carry out the pyrolysis process. About 20 g of SD was placed in a crucible with a lid, heated for two hours at 600°C in a muffle furnace, and then allowed to cool at room temperature. After removing ash and inorganic salts with dilute HCl, the resulting biochar was cleaned with deionised water and dried at 100°C.

$ZnCl_2$ was used to chemically activate the biochar, producing activated carbon. The impregnation ratio of $ZnCl_2$ to biochar was 1:1. After dissolving 10 g of $ZnCl_2$ in 150 mL of distilled water, 10 g of biochar was added to the mixture. The mixture was allowed to stand at room temperature for six hours. After filtering the liquid portion, the remaining solids were dried in a hot oven set to 110°C for approximately 24 hours. About 10 g of impregnated biochar was placed in a lidded crucible. ZnBC (zinc biochar) was the name given to the activated carbon produced under the optimised operating conditions. Finally, the biochar was washed with dilute HCl and then with distilled water until the pH of the filtrate reached a constant value. After drying, the sample was stored in a tightly sealed container for dye treatment. (Nirmaladevi & Palanisamy 2021).

SEM–EDS and TEM were used to examine the composite's morphological characteristics. XRD was used to determine the composite's crystalline structure. FTIR (Fourier transform infrared) spectroscopy was used to identify the composite's basic functional groups.

The adsorption models were examined using methylene blue (MB), a model organic pollutant obtained from the Merck Group. A stock solution (1000 mg L^{-1}) was prepared by dissolving 1000 mg of MB in 1.0 L of distilled water. MB solutions were prepared at concentrations of 100, 150, 200, 250, and 300 mg L^{-1}. Using 0.010 M NaOH and/or HCl solutions, the pH values of the MB solutions were adjusted to 2, 4, 6, 8, and 10. A temperature-controlled shaker bath was

used to hold containers containing the mixture of adsorbent particles and adsorbate molecules at 25 °C. The following formula was used to determine the MB adsorption capacity (q_e) from the residual MB concentration:

$$\text{Adsorption efficiency (\%)} = \frac{Ci-Ce}{Ci} \times 100$$

$$\text{Adsorption capacity } (q_e) = \frac{Ci-Ce}{m} \times v$$

Where V is the volume of the solution, and m is the amount of composite used.

When the adsorption tends to equilibrium, the adsorption capacity and the remaining MB concentration are indicated by q_e and C_e, respectively".

RESULTS AND DISCUSSION

To determine which functional groups were present on the adsorbent's surface, FTIR spectroscopy was employed (Fig.1). Cellulose and hemicellulose appear to be the primary constituents in the FTIR spectra shown in Fig. 1. The FTIR spectrum revealed key functional groups in the adsorbent material. A strong absorption peak at 3354 cm^{-1} corresponds to O–H stretching vibrations of hydroxyl groups. The peak at 1745 cm^{-1} is attributed to C=O stretching from carboxylic groups in hemicellulose. A distinct band at 1516 cm^{-1} arises from –CH bending vibrations in cellulose, while the absorption at 1392 cm^{-1} is associated with C–O stretching and CH/OH bending in hemicellulose. The peak at 1039 cm^{-1} represents C–O, C–O–H, C–O–C, and ring vibrations in cellulose and hemicellulose. Finally, the band at 677 cm^{-1} suggests aromatic bending modes in cellulose (Mosoarca et al. 2021).

The XRD results for ZnO@SD are displayed in Fig. 2. Diffraction peaks were observed at 32.74°, 33.49°, 36.57°, and 55.87°, according to the XRD pattern analysis. The FWHM (full width at half maximum) data reported in the corresponding journals showed that the crystalline peaks of ZnO nanoparticles matched the JCPDS card in the 36–1451 range. Upon closer examination, ZnO exhibited comparable properties and behaviour in the range of $20° < 2\theta < 80°$. In addition to being pure and devoid of impurities, the synthesised nanopowder showed no distinctive XRD peaks other than the observed ZnO peaks (Aigbe & Kavaz 2021).

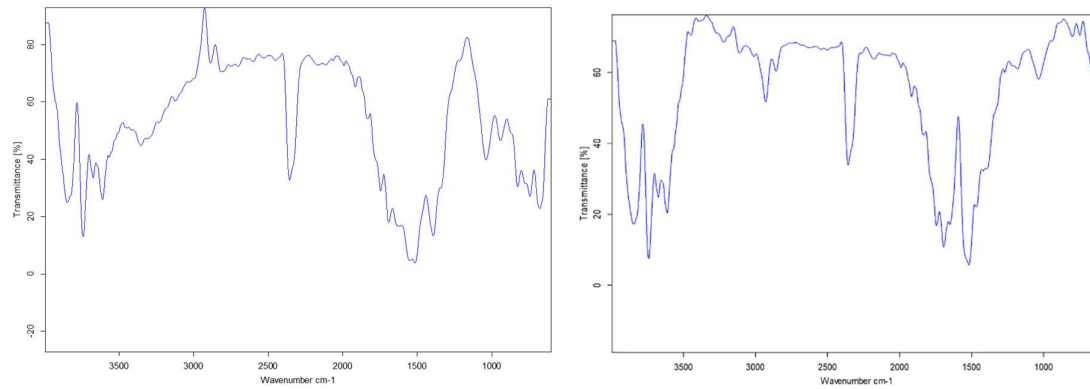

Fig. 1: FTIR spectrum of ZnO@SD before and after adsorption.

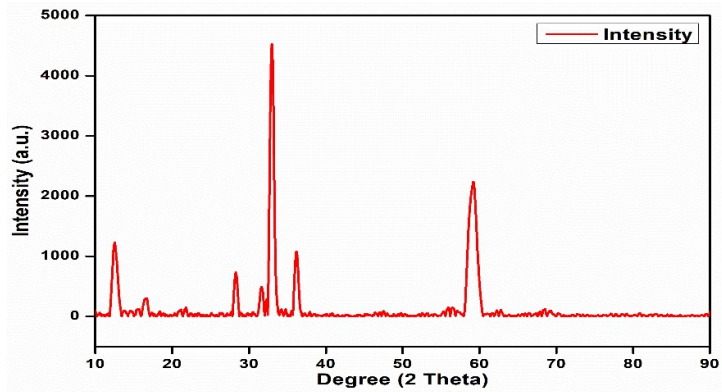

Fig. 2: XRD spectrum of ZnO@SD.

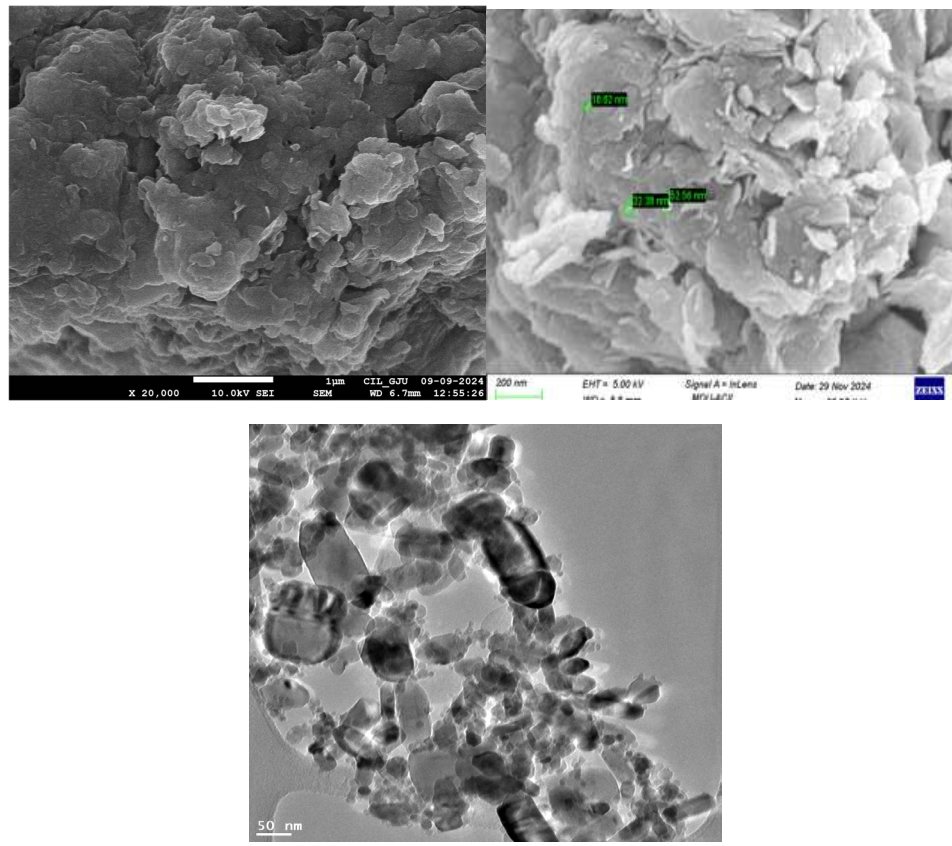

Fig. 3: SEM micrograph before and after MB adsorption, and TEM of ZnO@SD.

Fig. 3 displays ZnO@SD SEM images, which depict that the composite was found to have fewer uniform structures. In general, it can be stated that the addition of carbonized-sawdust composite altered the nanoparticles' surface morphology. The surface, which had a uniform structure and fewer cracks, became uneven. The nano-crystallites with large surface area and a strong propensity to aggregate, although the composite showed these aggregations more clearly (Aigbe et al. 2021). Multiple layers of particle arrangements are also visible, which raises the possibility of a high adsorption capacity.

The TEM image shows the porosity and surface texture of the adsorbent. It exhibited spherical surface coverage with rough, cracked surfaces and minuscule cavities. The morphology of the particles determines their suitability for adsorption. The image shows considerable roughness and a crisp texture that could enhance adsorption, and several pores are clearly visible on the surface. Extended fibrous particles and well-formed pores appear to result from the porous structure. The elemental composition of ZnO@SD nanoparticles is displayed in the EDX spectroscopy pattern in Fig. 4, which shows comparable peaks for each of the characterized samples. The patterns indicated that ZnO@SD nanoparticles had no elemental impurities and were primarily composed of Zn (8.1%), O (45.3%), and C (46.6%). The majority of organic contaminants in the sawdust biomass sample appear to have been broken down by carbonization. The EDX composition of ZnO@SD, synthesized and after MB adsorption, is displayed in Fig. 4, where Zn and O were the main compositional elements, with atomic percentages of C 73.3%, O 21.2%, and Zn 1.6%.

The adsorption of MB dye onto ZnO@SD was highly dependent on the composite's surface charge distribution and the pH of the solution. The pH of the solution affected the electrostatic interactions, which could be either repulsive or attractive, between the active sites on the surface of the composite and the MB dye species. The effect of changing the solution pH on MB dye adsorption is depicted in Fig. 5. It was found that the percentage of MB dye ions sorbed onto ZnO@SD increased significantly as the solution pH was changed from 2.0 to 12.0, with pH 6.0 showing the highest percentage removal of MB dye ions.

Since surface sites on ZnO@SD suggest the presence of significantly more negatively charged groups at low pH,

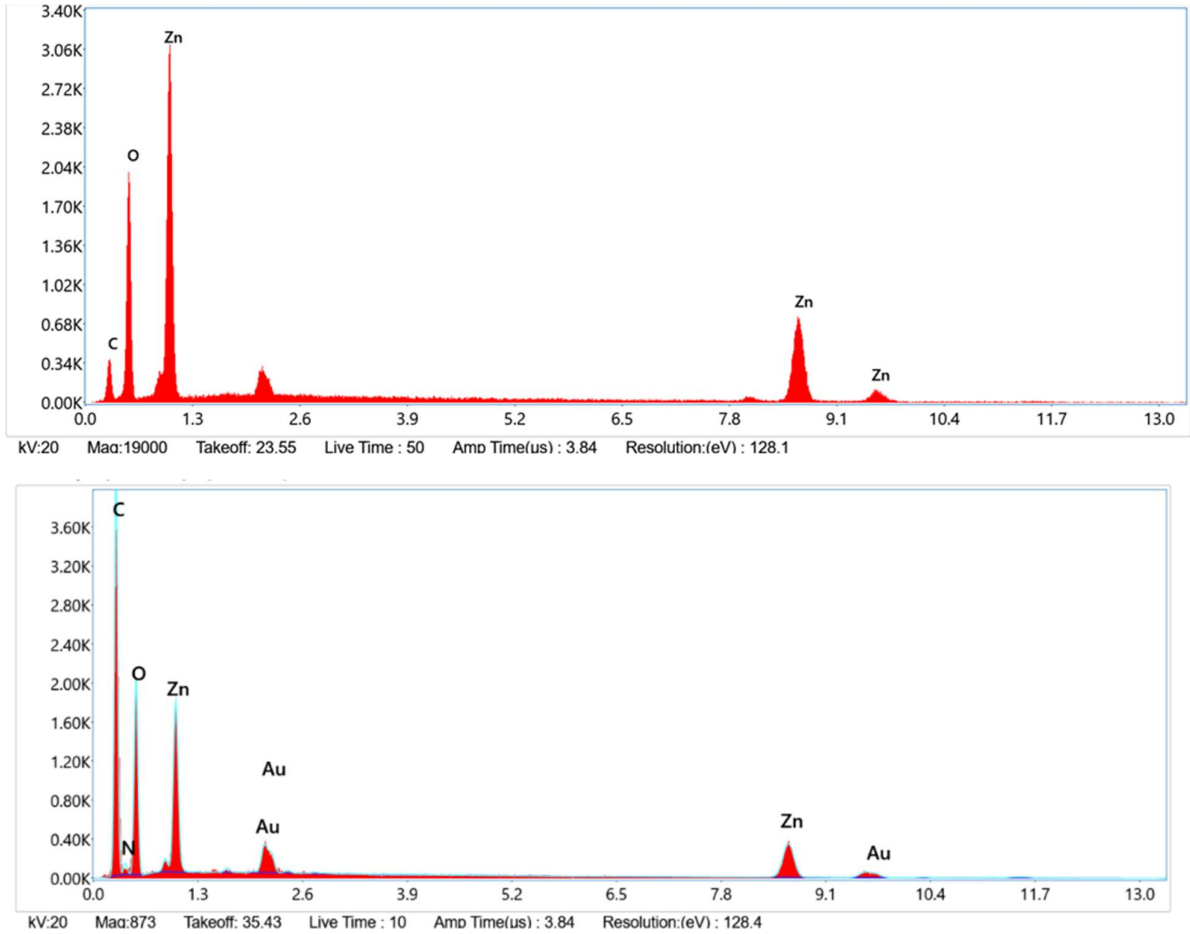

Fig. 4: EDS spectrum of ZnO@SD before and after adsorption of MB.

the lower percentage of MB dye adsorbed onto ZnO@SD at pH 2 was attributed to electrostatic repulsion between the negative surface charges and the cationic, undissociated MB species. Additionally, the percentage of MB dye removed at acidic pH decreased due to increased competition between MB^+ ions and H^+/H_3O^+ ions for biochar adsorption sites. At low pH values, interactions such as hydrogen bonding, π-π or π^+-π interactions, and pore diffusion were responsible for the adsorption of MB dye onto ZnO@SD (Phuong et al. 2019).

The improved percentage of MB dye removal at higher pH was attributed to electrostatic attraction between the dominant MB dye species and the increasingly negative surface charges as the solution pH increased. It has been reported that raising the pH of the solution increases the number of hydroxyl (-OH) and carboxylate ($-COO^-$) groups on the ZnO@SD surface, which in turn increases the number of negatively charged sites (Phuong et al. 2019). Studies by Phuong et al. (2019) and Al-Ghouti & Al-Absi (2020) revealed a similar pattern. The primary sorption mechanisms of MB dye at acidic and basic pH were hypothesized to be electrostatic interactions and hydrogen bonding (Al-Ghouti & Al-Absi 2020, Eldeeb et al. 2024).

Since it regulates the adsorption performance in the efficient removal of contaminants, the adsorbent dosage is an important parameter. The experiment used doses of ZnO@SD ranging from 10 mg to 80 mg. When the adsorbent dosage is increased from 10 mg to 70 mg, the percentage removal using ZnO@SD improves from 74.5 to 96.3% at equilibria (Fig. 5). Increased surface area and more binding sites for adsorption are the causes of the sorbate's constant improvement in percentage uptake with adsorbent dose. Nevertheless, an opposing trend in adsorption capacity was noted, as shown in Fig 5. The maximum adsorption capacity of 372.5 $mg.g^{-1}$ for M.B. by the adsorbent was noted at the lowest adsorbent dose. In light of this, it is important to note that adsorbent particles interact through amalgamation and aggregation at higher doses, resulting in a decrease in effective surface area per unit weight of adsorbent. It could

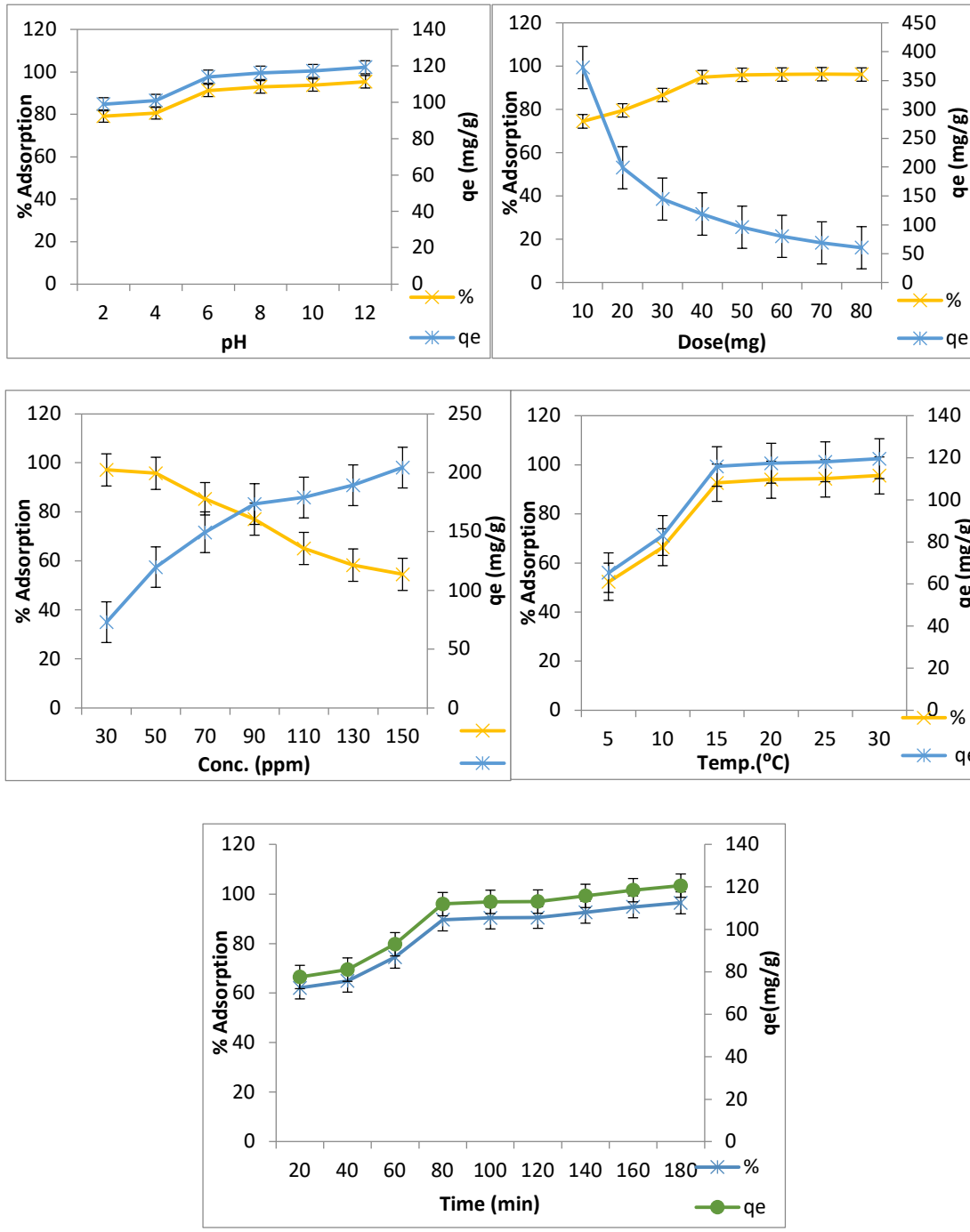

Fig. 5: Effect of pH of solution, adsorbent dosage, initial dye concentration, temperature and time on removal %age and adsorption capacity.

be explained by an increase in the adsorbent's surface area and an enhancement in accessibility of more active surface sites on the sorbent (Garg et al. 2004).

On the other hand, as the dose is increased, the adsorption capacity continuously and significantly decreases. Adsorbent particle interactions, such as agglomeration and aggregation, cause the adsorption capacity to decrease as the sorbent dose increases. As a result, the adsorbents' total surface area per unit weight decreases.

Methylene Blue (MB) dye adsorption tests were performed at various contact durations ranging from 20 to 180 min with an initial MB concentration of 50 ppm to

examine the adsorption kinetics. The effects of contact time on adsorption efficiency were examined at 298 K, 40 mg, and 6 pH. As contact time increased to 80 minutes removal %age rose to 89.56%, and the adsorption finally reached equilibrium. Fig. 5 shows how the initial MB concentration affected adsorption efficiency. There were sporadic variations in the curves of different starting concentrations. As the MB concentration ranged from 10 to 150 mg.L^{-1}, the highest adsorption efficiency of 97.13% at 30 ppm was noted.

The persistent active sites found it difficult to bind the increasing MB molecules from the bulk solution, even though there were enough active sites to explain the results at low initial MB dye concentrations. At higher methylene blue (MB) concentrations, increased electrostatic repulsion between dye cations reduced the adsorption efficiency. However, elevating the initial MB concentration also enhanced the adsorption capacity of the ZnO@SD composite. This occurred because a higher dye concentration provided a stronger driving force, helping to overcome mass transfer resistance between the aqueous phase and the adsorbent surface.(Hassaan et al. 2023).

Adsorption isotherm modeling can be used to describe the interaction of dye molecules with the sorbent at solid/liquid interfaces. Three isotherm models—the Langmuir, Freundlich, and Temkin models—were applied to the experimental data of dye adsorption at different dye concentrations (10–150 mg.L^{-1}). The Langmuir isotherm model is based on the assumption that adsorption occurs in a monolayer, where dye molecules bind to a finite number of identical and energetically equivalent active sites on the adsorbent surface. This model also presumes that no interactions occur between adsorbed molecules (Langmuir 1916). In contrast, the Freundlich isotherm model is an empirical equation that describes multilayer adsorption on a heterogeneous surface with non-uniform binding sites. Unlike the Langmuir model, it does not assume a saturation limit, implying an infinite number of active sites with varying adsorption energies (Freundlich 1906). According to the Temkin model, the adsorbate's heat of adsorption decreases linearly with monolayer coverage, and the surface has an even distribution of active binding sites (Temkin & Pyzhev 1940). The models' linear plots are displayed in Fig. 6. Table 1 summarizes the calculated regression coefficients and

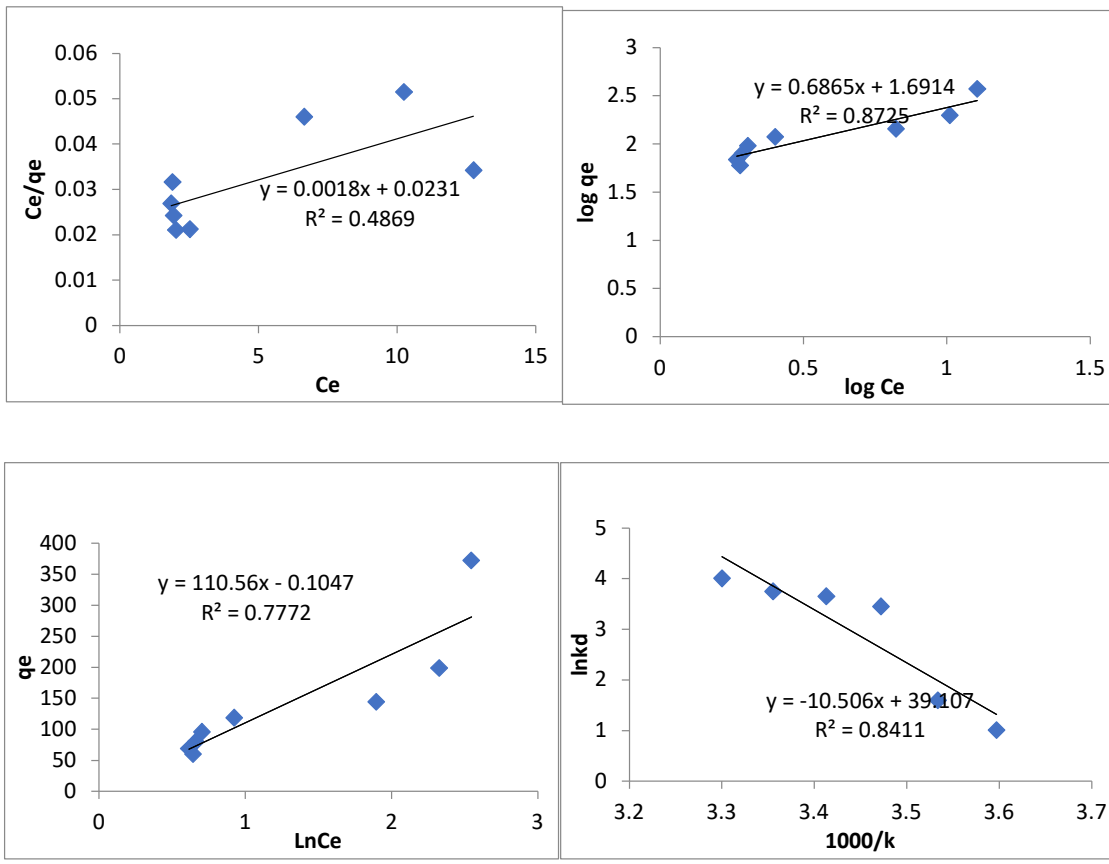

Fig. 6: Isotherms: Langmuir, Freundlich and Temkin, and Vant Hoff plot.

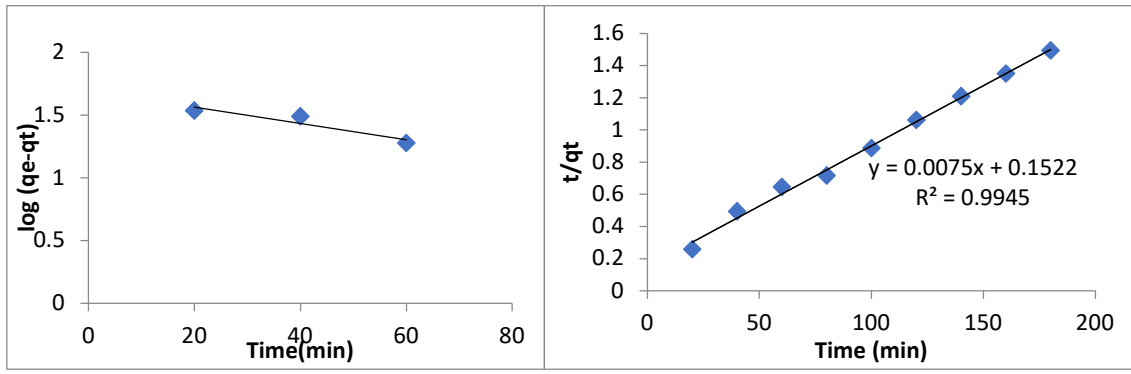

Fig. 7: Kinetics study.

isotherm parameters for each model using the corresponding linear plots. Each model's regression coefficient and isotherm parameters were used to determine its applicability to the dye adsorption experiments. The comparison revealed that the Freundlich model best described the MB dye adsorption process, indicating that MB dye molecules were adsorbed in multiple layers onto the heterogeneous surface-active sites.

For MB dye, the Freundlich model's R^2 was determined to be 0.87. The fact that the 1/n (slope) value ranged from 0 to 1, or 0.686 for MB, suggests that adsorption was favorable and that the dye molecules chemically bonded to the adsorbent surface, indicating chemisorption. A 1/n value less than 1 indicates chemisorption on the adsorbent's heterogeneous surface. The MB dye's R^L value was found to be 0.206 ($0 < R^L < 1$), confirming a favorable adsorption process. It was observed that MB dye had a maximum monolayer adsorption capacity (q_m) of 555.5 mg.g^{-1}, while the experimental value was 372.5 mg.g^{-1}. Consequently, the chemisorption of dye molecules onto ZnO@SD was validated by the isotherm models.

Temperature ranges of 278–303 K were examined because thermodynamic research offers more details regarding the adsorption mechanism of ZnO@SD on MB. The van't Hoff equation was used to calculate all thermodynamic parameters, including enthalpy (ΔH), entropy change (ΔS), and the standard Gibbs free energy (ΔG), which showed how the equilibrium constant depended on temperature. The equilibrium constant (K) was determined from the adsorption isotherm data using the following equation:

$K = q_e/C_e$, while the positive value of ΔS° (0.325 kJ.moL^{-1} K^{-1}) indicated that the randomness at the solid/solution interface increased, and the positive value of enthalpy ΔH° (87.29 kJ.moL^{-1}), one of the thermodynamic parameters shown in Table 1, confirmed that the adsorption of MB onto ZnO@SD was endothermic in nature. This was because the adsorbate ions lost less transitional energy than the water molecules displaced by the adsorbate species. The adsorption mechanism of MB onto the ZnO@SD nanocomposite was a favorable, spontaneous process, as indicated by the negative values of ΔG°. Enthalpy values ΔH° < 84 kJ.moL^{-1} indicate physisorption, while values between 84 and 420 kJ.moL^{-1} indicate chemisorption. The observed value of 87.29 kJ.moL^{-1} suggests chemisorption, placing it on the borderline between physisorption and chemisorption. Multilayer adsorption or pore-filling mechanisms (physisorption) may be possible, along with the potential

Table 1: Isotherms, thermodynamics and kinetics.

	Parameters	Values
Langmuir	q_m	555.5
	B	0.077
	R_L	0.206
	R^2	0.48
Freundlich	1/n	0.686
	K_f	48.97
	R^2	0.87
Temkin	A_T	1.00
	R^2	0.77
Thermodynamics	ΔS°	0.325
	ΔH°	87.29
	ΔG° 278K	-1.67
	ΔG°283K	-3.27
	ΔG°288K	-4.87
	ΔG°293K	-6.47
	ΔG°298K	-8.07
	ΔG°303K	-9.67
PFO	q_e	1.01
	K1	3.89
	R^2	0.87
PSO	q_e	133.33
	K2	0.00037
	R^2	0.99

involvement of strong chemical interactions (ligand exchange, complexation) supporting chemisorption. The influence of temperature on the adsorption mechanism is noted, as higher ΔH° values often correlate with chemisorption but may also reflect high-energy physical adsorption. Consequently, the results suggest that chemical interaction may be the primary mechanism underlying the sorption of MB onto ZnO@SD.

Pseudo-first-order rate kinetics and pseudo-second-order rate kinetics models were used to further study the adsorption phenomenon, and Table 1 summarizes the parameters that were obtained. Table 1 shows that the kinetics of MB adsorption onto ZnO@SD nanocomposite are described by the pseudo-second order rate kinetics model. In comparison to the pseudo-first-order model, the linear regression values derived from this model yielded a higher correlation coefficient (R^2) of >0.99. The model's suitability for describing the adsorption process is further supported by the observation of linear curves in Fig. 7, which also shows fitment to pseudo-second order. It's possible that the methylene blue interaction with the adsorption site was chemical in nature because the adsorption process adheres to the pseudo-second-order model.

It was proposed that chemical adsorption played a role in achieving the highest MB adsorption from simulated water, given the scale used in the linearized form of the pseudo-second-order model. Pseudo-second-order kinetics was also used to model the early stage of kinetic experimental data to verify this (Fig. 7). Based on this evidence, the adsorption kinetics of MB onto ZnO@SD nanocomposite are primarily diffusion-based mechanisms. During a rate-limiting mechanistic step, various adsorption sites on a homogeneous solid substrate randomly collide with one another and diffuse through the adsorbent pore size.

CONCLUSIONS

Sawdust is a cheap and plentiful lignocellulosic material that is a bio-waste product of industry and agriculture. In this study, mixed sawdust was used as the raw material to produce ZnO@SD adsorbent. ZnO@SD has a network structure and works well as an adsorbent for cationic dyes because it has a lot of amino, hydroxyl, and carboxyl groups. ZnO@SD can be used to adsorb cationic dye MB in water and has a favorable separation capacity, high removal rate, and good adsorption capacity. The aforementioned processes are well-fitted by the Freundlich adsorption isotherm and the pseudo-second-order kinetic model. ZnO@SD's easy preparation method and superior adsorption capabilities. This work offers useful ZnO@SD adsorbents for the elimination of cationic dyes from wastewater. It is a low-cost bio-waste sawdust, which is a sustainable, scalable, and environmentally friendly method that can show great promise for a variety of additional uses in the future.

ACKNOWLEDGMENTS

The authors are thankful to DCRUST, Murthal, for providing facilities for the research.

REFERENCES

Ahamad, Z. and Nasar, A., 2024. Synthesis, characterization, and application of magnetized Azadirachta indica sawdust as a novel adsorbent: Kinetic and isotherm studies in removing methylene blue as a model dye. *Cellulose*, 31(6), pp.3763-3782.

Aigbe, R. and Kavaz, D., 2021. Unravel the potential of zinc oxide nanoparticle-carbonized sawdust matrix for the removal of lead (II) ions from aqueous solution. *Chinese Journal of Chemical Engineering*, 29, pp.92-102.

Aigbe, R., Akhayere, E., Kavaz, D. and Akiode, O.K., 2021. Characteristics of zinc oxide and carbonized sawdust nanocomposite in the removal of cadmium (II) ions from water. *Water, Air, & Soil Pollution*, 232, pp.1-19.

Al-Ghouti, M.A. and Al-Absi, R.S., 2020. Mechanistic understanding of the adsorption and thermodynamic aspects of cationic methylene blue dye onto cellulosic olive stones biomass from wastewater. *Scientific Reports*, 10(1), p.15928.

Bo, L., Gao, F., Bian, Y., Liu, Z. and Dai, Y., 2021. A novel adsorbent, Auricularia Auricular for the removal of methylene blue from aqueous solution: Isotherm and kinetics studies. *Environmental Technology & Innovation*, 23, p.101576.

Bulgariu, L., Escudero, L.B., Bello, O.S., Iqbal, M., Nisar, J., Adegoke, K.A. and Anastopoulos, I., 2019. The utilization of leaf-based adsorbents for dyes removal: A review. *Journal of Molecular Liquids*, 276, pp.728-747.

Cao, V., Cao, P.A., Han, D.L., Ngo, M.T., Vuong, T.X. and Manh, H.N., 2024. The suitability of Fe3O4/graphene oxide nanocomposite for adsorptive removal of methylene blue and Congo red. *Nature Environment and Pollution Technology*, 23(1), pp.255-263.

Dutta, S., Gupta, B., Srivastava, S.K. and Gupta, A.K., 2021. Recent advances on the removal of dyes from wastewater using various adsorbents: A critical review. *Materials Advances*, 2(14), pp.4497-4531.

Eldeeb, T.M., Aigbe, U.O., Ukhurebor, K.E., Onyancha, R.B., El-Nemr, M.A., Hassaan, M.A. and El Nemr, A., 2024. Adsorption of methylene blue (MB) dye on ozone, purified and sonicated sawdust biochars. *Biomass Conversion and Biorefinery*, 14(8), pp.9361-9383.

Freundlich, H.M.F., 1906. Over the adsorption in solution. *Journal of Physics and Chemistry*, 57(385471), pp.1100-1107.

Garg, V.K., Amita, M., Kumar, R. and Gupta, R., 2004. Basic dye (methylene blue) removal from simulated wastewater by adsorption using Indian Rosewood sawdust: A timber industry waste. *Dyes and Pigments*, 63(3), pp.243-250.

Hassaan, M.A., Yılmaz, M., Helal, M.A.M., Ragab, S. and El Nemr, A., 2023. Isotherm and kinetic investigations of sawdust-based biochar modified by ammonia to remove methylene blue from water. *Scientific Reports*, 13(1), pp.1-20.

Khan, I., Saeed, K., Zekker, I., Zhang, B., Hendi, A.H., Ahmad, A. and Khan, I., 2022. Review on methylene blue: Its properties, uses, toxicity and photodegradation. *Water*, 14(2), p.242.

Langmuir, I., 1916. The constitution and fundamental properties of solids and liquids. Part I. Solids. *Journal of the American Chemical Society*, 38(11), pp.2221-2295.

Mosoarca, G., Popa, S., Vancea, C. and Boran, S., 2020. Optimization, equilibrium and kinetic modeling of methylene blue removal from aqueous solutions using dry bean pods husk powder. *Materials*, 14(19), p.5673.

Nirmaladevi, S. and Palanisamy, P.N., 2021. Adsorptive behavior of biochar and zinc chloride activated hydrochar prepared from Acacia leucophloea wood sawdust: Kinetic equilibrium and thermodynamic studies. *Desalination and Water Treatment*, 209, pp.170-181.

Phuong, D.T.M., Loc, N.X. and Miyanishi, T., 2019. Efficiency of dye adsorption by biochars produced from residues of two rice varieties, Japanese Koshihikari and Vietnamese IR50404. *Desalination and Water Treatment*, 165, pp.333-351.

Pimental, C.H., Freire, M.S., Gómez-Díaz, D. and González-Álvarez, J., 2023. Preparation of activated carbon from pine (Pinus radiata) sawdust by chemical activation with zinc chloride for wood dye adsorption. *Biomass Conversion and Biorefinery*, 13(18), pp.16537-16555.

Prodjosantoso, A.K., Nurul Hanifah, T.K., Utomo, M.P., Budimarwanti, C. and Sari, L.P., 2025. The synthesis of AgNPs/SAC using banana frond extract as a bioreducing agent and its application as a photocatalyst in methylene blue degradation. *Nature Environment & Pollution Technology*, 24(1).

Sayed, N.S., Ahmed, A.S., Abdallah, M.H. and Gouda, G.A., 2024. ZnO@ activated carbon derived from wood sawdust as an adsorbent for the removal of methyl red and methyl orange from aqueous solutions. *Scientific Reports*, 14(1), pp.1-18.

Temkin, M.J. and Pyzhev, V., 1940. Recent modifications to Langmuir isotherms. *Journal of Physical Chemistry*, 10(2), pp.183-192.

Yadav, S., Bajar, S., Hemraj, et al., 2023. Assessment of groundwater quality near municipal solid waste landfill by using multivariate statistical technique and GIS: A case study of Bandhwari (Gurugram) landfill site, Haryana, India. *Sustainable Water Resources Management*, 9, p.174.

Yadav, S., Rohilla, R. and Chhikara, S.K., 2024a. Review on landfill leachate treatment: Focus on the applicability of adsorbents. *Proceedings of the National Academy of Sciences, India, Section B: Biological Sciences*, 94(2), pp.123-136.

Yadav, S., Yadav, A., Goyal, G., Dhawan, M., Kumar, V., Yadav, A., Dhankhar, R., Sehrawat, N. and Chhikara, S.K., 2024b. Fly ash-based adsorption for hexavalent chromium removal in aqueous systems: A promising eco-friendly technique. *Oriental Journal of Chemistry*, 40(1), pp.182-196.

Zafar, M.N., Dar, Q., Nawaz, F., Zafar, M.N., Iqbal, M. and Nazar, M.F., 2019. Effective adsorptive removal of azo dyes over spherical ZnO nanoparticles. *Journal of Materials Research and Technology*, 8(1), pp.713-725.

Zhang, F., Chen, X., Wu, F. and Ji, Y., 2016. High adsorption capability and selectivity of ZnO nanoparticles for dye removal. *Colloids and Surfaces A: Physicochemical and Engineering Aspects*, 509, pp.474-483.